# A Pedigree-Based Map of Crossovers and Noncrossovers in Aye-Ayes (*Daubentonia madagascariensis*)

Cyril J. Versoza[1,†], Audald Lloret-Villas[1,†], Jeffrey D. Jensen [1], Susanne P. Pfeifer [1,*]

[1]Center for Evolution and Medicine, School of Life Sciences, Arizona State University, Tempe, AZ, USA

*Corresponding author: E-mail: susanne@spfeiferlab.org.

[†]These authors contributed equally to this work.

**Accepted:** April 10, 2025

## Abstract

Gaining a better understanding of the rates and patterns of meiotic recombination is crucial for improving evolutionary genomic modeling, with applications ranging from demographic to selective inference. Although previous research has provided important insights into the landscape of crossovers in humans and other haplorrhines, our understanding of both the considerably more common outcome of recombination (i.e. noncrossovers) as well as the landscapes in more distantly related primates (i.e. strepsirrhines) remains limited owing to difficulties associated with both the identification of noncrossover tracts as well as species sampling. Thus, in order to elucidate recombination patterns in this understudied branch of the primate clade, we here characterize crossover and noncrossover landscapes in aye-ayes utilizing whole-genome sequencing data from six three-generation pedigrees and three two-generation multi-sibling families, and in so doing provide novel insights into this important evolutionary process shaping genomic diversity in one of the world's most critically endangered primate species.

**Key words:** recombination, primate, strepsirrhine, Daubentoniidae, population genomics.

## Significance

The rates of recombination—a fundamental process in mammalian meiosis—differ markedly between species. In this study, we provide the first recombination rate estimates for a strepsirrhine, the aye-aye (*Daubentonia madagascariensis*)—a highly endangered species and valuable comparative outgroup for future primate studies.

## Introduction

Recombination is a fundamental biological process required for faithful gametogenesis in most sexually reproducing species (see the reviews of Baudat et al. (2013) and Johnston (2024)). Apart from being essential for the proper pairing of homologous chromosomes and their segregation into gametes during meiosis (Keeney 2001), recombination also plays an important evolutionary role in shuffling genetic variation, improving the efficacy of natural selection by breaking linkage interference between segregating beneficial and deleterious alleles (Hill and Robertson 1966; Felsenstein 1974; and see the review of Charlesworth and Jensen (2021)).

In primates, as in many other organisms, meiotic recombination predominantly occurs in 1 to 2 kb long regions of the genome—so-called recombination "hotspots"—the location of which is mainly determined by the zinc-finger protein PRDM9 (Baudat et al. 2010; Myers et al. 2010; Parvanov et al. 2010). By binding specific DNA sequence motifs and trimethylating histone H3 at lysines 4 and 36 (Powers et al. 2016), PRDM9 guides the meiotic machinery

to initiate the formation of DNA double-strand breaks, the repair of which may result in either a reciprocal exchange between homologs (termed a crossover; CO) or a unidirectional replacement of a genomic region in one chromosome leaving the donor homolog unmodified (termed a noncrossover; NCO) (see the reviews of Wang et al. (2015), Lorenz and Mpaulo (2022), and Johnston (2024)).

While both COs and NCOs play important roles in shaping genetic diversity (Przeworski and Wall 2001), previous studies have suggested that NCOs tend to be considerably more common than COs in most organisms (Jeffreys and May 2004; Cole et al. 2010; Comeron et al. 2012; Li et al. 2019; Palsson et al. 2025). However, owing to the difficulty in detecting the often very small NCO events (with most tract lengths in humans being <1 kb; Jeffreys and May 2004; Williams et al. 2015; Halldorsson et al. 2016; Palsson et al. 2025), combined with the need for a segregating variant to be present in the donor homolog in order to allow identification (i.e. the tract remains undetectable if the donor and converted sequence are identical), the NCO landscape remains comparatively understudied. For these same reasons, combined with other underlying assumptions such as geometrically distributed tract lengths, computational approaches for NCO inference are generally characterized by poor accuracy (see discussion of Wall et al. (2022)). As such, time-consuming and costly direct pedigree-sequencing studies remain the most promising avenue for improving our understanding of this process (and see Peñalba and Wolf (2020) for a detailed overview of current methodologies).

With regards to primates specifically, although previous research has begun to elucidate the rates and patterns of recombination in haplorrhines—a suborder of primates that includes humans (Kong et al. 2002, 2010; Coop et al. 2008; Pratto et al. 2014; Williams et al. 2015; Halldorsson et al. 2016; Palsson et al. 2025), other great apes (Auton et al. 2012; Pfeifer and Jensen 2016; Stevison et al. 2016), and monkeys (Rogers et al. 2000, 2006; Cox et al. 2006; Jasinska et al. 2007; Xue et al. 2016, 2020; Pfeifer 2020; Wall et al. 2022; Versoza et al. 2024b)—little remains known about this process in strepsirrhines (though see Soni et al. 2024). As the most basal suborder of primates, gaining insights into the population genetic forces shaping the genomes of strepsirrhines is crucially important, not only to improve our understanding of primate evolution, but also for elucidating the scale at which recombination rates and spatial distributions of CO and NCO events may change between taxonomic groups, as this variation has been shown to be substantial (see the reviews of Paigen and Petkov (2010) and Stapley et al. (2017)). Given the vital role of recombination in maintaining genetic diversity, such inference is additionally important for the development of effective conservation strategies, particularly as many strepsirrhines are highly endangered (Gross 2017). For example, among the more than 100 species of strepsirrhines endemic to Madagascar (Mittermeier et al. 2010), aye-ayes (*Daubentonia madagascariensis*) are one of the most threatened by anthropogenic activities, such as slash-and-burn agriculture, logging, mining, and urbanization (Suzzi-Simmons 2023), with the resulting extensive habitat loss and fragmentation having already decimated their populations to an estimated 1,000 to 10,000 individuals (Louis et al. 2020).

Thus, to elucidate the rates and patterns of recombination in this understudied branch of the primate tree—which represents an early split in the primate clade and thus a valuable comparative outgroup for future primate studies—we here investigate both the more commonly studied CO and the less-commonly studied NCO landscapes in aye-ayes. Using whole-genome sequencing data from six three-generation pedigrees and three (partially overlapping) two-generation multi-sibling families, we present the first recombination rate estimates for a strepsirrhine and thereby provide novel insights into this important evolutionary process shaping genetic diversity in one of the world's most critically endangered primate species.

## Results and Discussion

To study the rates and patterns of recombination in aye-ayes, 14 individuals were selected from a multi-generation pedigree housed at the Duke Lemur Center, the genomes of which were sequenced to mean depths of 50× (supplementary table S1, Supplementary Material online; Versoza et al. 2025). After mapping reads to the species-specific genome assembly (Versoza and Pfeifer 2024), autosomal variants were called following the Genome Analysis Toolkit's Best Practices (van der Auwera and O'Connor 2020), and filtered using a set of coverage-, genotype-, and inheritance-based criteria, resulting in a high-confidence call set consisting of 1.8 million variants (supplementary table S2, Supplementary Material online). For the purpose of this study, this call set from a multi-generation pedigree was divided into partially overlapping six three-generation pedigrees and three two-generation nuclear families with multiple offspring (supplementary fig. S1, Supplementary Material online) for which gamete transmission could be tracked in order to identify recombination events based on "phase-informative" markers—that is, heterozygous variants for which the parent-of-origin could be determined (with an average of 0.5 million phase-informative markers per pedigree/family; supplementary table S3, Supplementary Material online, and see supplementary table S4 and figs. S2 to S15, Supplementary Material online for the marker density across each autosome per pedigree/family). Based on these phase-informative markers, recombination events were classified as either COs—that is, a single change of haplotype phase along a chromosome (from maternally inherited to paternally inherited haplotype blocks or vice

versa)—or NCOs—that is, phase-informative markers that mismatched surrounding haplotype blocks (for additional details, see "Materials and Methods").

## The Landscape of COs in Aye-Ayes

A total of 119 and 308 putative CO events were identified across the autosomes in 6 and 18 meioses through the pedigree-based approach and the family-based approach, respectively. Visual inspection of these initial datasets revealed a clustering (i.e. ≥2 COs originating from the same meiosis located within <1 Mb) of 40 COs across 8 genomic regions, with the majority of these events (90%) identified through only one of the two approaches (supplementary table S5, Supplementary Material online). Although COs form at random during meiosis, CO interference tightly regulates their location within each chromosome (Muller 1916; Broman and Weber 2000), making such a pattern highly implausible in nature (see the discussions of Wall et al. (2022) and Versoza et al. (2024b)). More likely, these observations are driven by localized genotyping errors; thus, these CO events were excluded from further analyses, as is common practice. Subsequently, pedigree-based and family-based datasets were manually consolidated across the 20 meioses by removing duplicate recombination events observed in the four meioses that could be studied using both approaches (i.e. the meioses for the focal individual—offspring pairs 7–12, 7–13, 8–12, and 8–13; see supplementary fig. S1, Supplementary Material online), yielding a set of 324 distinct CO events. Thereby, the majority of consolidated events (54%) shared identical start and end coordinates at the break point; in cases of a partial overlap (i.e. a sharing of either start or end coordinates at the break point owing to differences in phase-informative markers in the two approaches), the CO events with the shortest resolution (i.e. the smallest region in which the CO could be located) were selected. Notably, CO events are supported by ~8,000 phase-informative markers on average and all CO events in the meioses that could be studied using pedigree-based and family-based approaches were also identified by both approaches, thus serving as a valuable validation of the employed methodology. After the datasets were consolidated, an additional 19 COs were removed either because the event was detected across multiple meioses (18 COs), possibly indicating a misplacement or inversion of a contig during the genome assembly, or because it occurred at the same position as an NCO in another individual (1 CO), thus likely resulting from a genotyping error (supplementary table S6, Supplementary Material online). The final dataset contained 305 COs: 163 and 142 COs in the 10 maternal and 10 paternal meioses, respectively (Fig. 1a; and see supplementary table S7, Supplementary Material online for the location of the observed events).

Aye-ayes exhibit one of the lowest levels of nucleotide diversity of any primate studied to date (Perry et al. 2013; Soni et al. 2025; Terbot et al. 2025b)—yet, despite this low marker density across the pedigree, the median resolution of male and female CO events (12.9 and 20.0 kb; supplementary fig. S16, Supplementary Material online, and see supplementary table S8, Supplementary Material online for a summary) is on par with those previously obtained from similarly sized nonhuman primate pedigree studies (7.7 and 22.3 kb in olive baboons [Wall et al. 2022] and rhesus macaques [Versoza et al. 2024b], respectively). In accordance with CO assurance, ensuring an obligate CO between homologous chromosomes (or chromosome arms) during meiosis (Jones and Franklin 2006), an average of 1.1 COs were identified per chromosome and meiosis. In total, between 10 and 21 COs were observed per meiosis across the 14 autosomes (supplementary table S8, Supplementary Material online), with CO densities in males and females roughly inversely correlated with chromosome size (supplementary fig. S17, Supplementary Material online).

In order to gain a better understanding of the nature of hotspots, information from CO events with a resolution of less than 10 kb was leveraged to search for putative sequence motifs of PRDM9 binding sites in aye-ayes. Application of a de novo motif finding algorithm (Bailey and Elkan 1994) allowed for the identification of a degenerate sequence motif present in these CO regions (Fig. 1b)—a motif that exhibits considerable similarities with PRDM9 binding motifs previously identified in humans (see Fig. 1a in Altemose et al. (2017) for zinc-finger domains 7 to 12), despite a high turn-over rate of PRDM9 binding motifs between species. CO events were significantly enriched in regions harboring this degenerate sequence motif compared with the genomic background (Fisher's exact test, $P$-value < 2.2e-16). Interestingly, AlphaFold 3 (Abramson et al. 2024) predicted an interaction between PRDM9 and the putative DNA binding motif in aye-ayes with high confidence (ipTM = 0.91, with a score close to 1.0 suggesting that the protein–DNA interface is well-defined), confirming PRDM9–DNA binding in silico. Visualization of the PRDM9–DNA complex further supports this prediction (Fig. 1c), showing well-folded C2H2 zinc-finger domains (with a very high-confidence score of pLDDT > 90) binding DNA at the discovered motif.

Consistent with a preferential binding of PRDM9 in intronic and intergenic regions that are often more accessible in chromatin structure (Coop et al. 2008; Walker et al. 2015), CO events were enriched in these genomic regions at the broad scale (supplementary fig. S18, Supplementary Material online). At the fine scale, the number of COs was considerably lower near, and higher farther away from, genes (supplementary fig. S19, Supplementary Material online)—an observation in agreement with previous studies showing that PRDM9 directs COs away from transcription start sites in primates (Myers et al. 2005; Coop et al. 2008; Auton et al. 2012). Additionally, a clustering of COs was observed toward the telomeric ends in males, while females

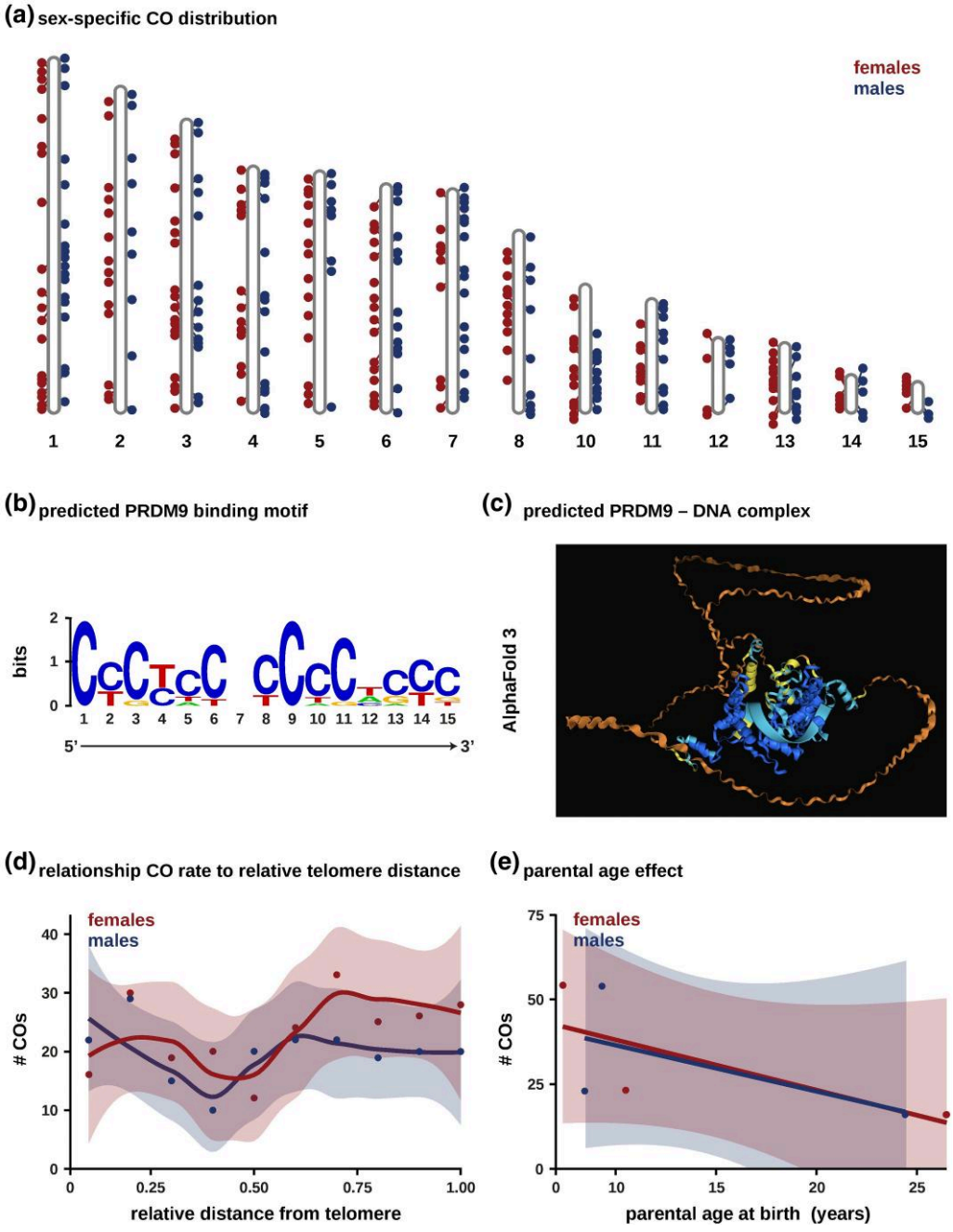


**Fig. 1. Characteristics of crossovers**. a) The genomic distribution of CO events in females (shown as red circles) and males (blue circles) across the autosomes (note that scaffold 9, i.e. chromosome X, is not displayed). b) Motif of the predicted PRDM9 binding sequence in aye-ayes. c) PRDM9—DNA complex predicted by AlphaFold 3 (Abramson et al. 2024). Colors indicate confidence (dark blue: very high, predicted local distance difference test [pLDDT] > 90; turquoise: confident, 90 > pLDDT > 70; yellow: low, 70 > pLDDT > 50; orange: very low, pLDDT < 50). Predictions are provided for noncommercial use only, under and subject to AlphaFold Server Output Terms of Use found at alphafoldserver.com/output-terms. d) Relationship between female and male CO rates and relative proximity to telomeric regions. e) Relationship between maternal and paternal age at birth and the number of CO events.

displayed an overall larger number of COs that were more evenly spaced throughout the genome (Fig. 1d), as previously observed in other primates (e.g. Kong et al. 2002, 2010; Coop et al. 2008; Wall et al. 2022; and see Lenormand and Dutheil 2005; Sardell and Kirkpatrick 2020 for a discussion of this widespread phenomenon). Moreover, in agreement with recent studies in humans (Porubsky et al. 2024) and chimpanzees (Venn et al. 2014), the frequency of CO events decreased with both maternal and paternal age in aye-ayes (with 1.48 and 1.36 fewer COs per year,

**Table 1** Number of CO events and genetic distances identified in maternal/paternal meioses

| Scaffold | Length (Mb) | # CO events | cM | cM/Mb |
|---|---|---|---|---|
| 1 | 316.17 | 20/18 | 200/180 | 0.63/0.57 |
| 2 | 290.59 | 14/9 | 140/90 | 0.48/0.31 |
| 3 | 261.42 | 18/14 | 180/140 | 0.69/0.54 |
| 4 | 219.69 | 13/14 | 130/140 | 0.59/0.64 |
| 5 | 215.45 | 14/8 | 140/80 | 0.65/0.37 |
| 6 | 204.02 | 16/13 | 160/130 | 0.78/0.64 |
| 7 | 199.60 | 9/16 | 90/160 | 0.45/0.80 |
| 8 | 162.77 | 11/9 | 110/90 | 0.68/0.55 |
| 10 | 114.90 | 12/10 | 120/100 | 1.04/0.87 |
| 11 | 102.08 | 9/10 | 90/100 | 0.88/0.98 |
| 12 | 67.30 | 4/5 | 40/50 | 0.59/0.74 |
| 13 | 62.73 | 11/8 | 110/80 | 1.75/1.28 |
| 14 | 34.25 | 6/5 | 60/50 | 1.75/1.46 |
| 15 | 28.26 | 6/3 | 60/30 | 2.12/1.06 |
| **Autosomal (sex-averaged)** | **2,279.23** | **163/142 (152.5)** | **1,630/1,420 (1,525)** | **0.94/0.77 (0.85)** |

respectively; Fig. 1e); however, given the small sample size, this observation is not statistically significant (maternal: adjusted $R^2 = 0.1307$, *P*-value: 0.4583 and paternal: adjusted $R^2 = -0.2682$, *P*-value: 0.5864). Based on the number of COs per meiosis, the sex-averaged autosomal genetic map was estimated to be 1,525 cM in length (Table 1)—approximately 25% to 35% shorter than those of catarrhines (Rogers et al. 2000, 2006; Cox et al. 2006; Jasinska et al. 2007; Wall et al. 2022; Versoza et al. 2024b) as may be anticipated from the lower karyotype ($2n = 30$ in aye-ayes [Tattersall 1982] vs. $2n = 42$ and 60 in rhesus macaques [Owen et al. 2016] and vervet monkeys [Finelli et al. 1999], respectively) (Pardo-Manuel de Villena and Sapienza 2001), which, in turn, exhibit shorter map lengths than hominoids (Kong et al. 2002, 2010; Venn et al. 2014). Similar to other primates, females exhibit an overall longer genetic map length than males (1,630 vs. 1,420 cM)—however, the ratio of the female to male autosomal map length (1.15) is lower than that observed in humans (1.36; Porubsky et al. 2024). The genome-wide average CO rates in males and females were thus estimated to be 0.77 and 0.94 cM/Mb (Table 1)—approximately 40% to 50% lower than the average rates of 1.3 and 2.0 cM/Mb reported in humans (Bhérer et al. 2017)—with the overall lower sex-averaged rate (0.85 cM/Mb) likely contributing to the low levels of genetic diversity observed in the species (Perry et al. 2013; Soni et al. 2025; Terbot et al. 2025b).

## The Landscape of NCOs in Aye-Ayes

After excluding both complex events (involving multiple, non-contiguous NCO tracts within <5 kb) and NCOs with tracts >10 kb which were previously shown to frequently represent incorrect genotype calls and/or assembly errors (Smeds et al. 2016; Wall et al. 2022), 145 and 191 putative NCO events were identified through the pedigree-based approach and the family-based approach, respectively. Given the partial overlap between the two-generation nuclear families and the three-generation pedigrees (supplementary fig. S1, Supplementary Material online), NCOs identified in meioses that could be studied using both approaches were subsequently consolidated into 287 distinct NCO events. Careful manual curation using highly stringent quality metrics removed 87 out of these 287 NCOs, either because the event was detected across multiple meioses (85 NCOs) or because the phase-informative markers overlapped with a structural variant in the same individual (1 NCO; Versoza et al. 2024a) or a CO in another individual (1 NCO) (for details, see supplementary table S9, Supplementary Material online). The final dataset thus contained 200 NCOs, 95 and 105 of maternal and paternal origin, respectively (Fig. 2a; and see supplementary table S10, Supplementary Material online for details). Notably, as expected from NCOs frequently localizing at the same recombination hotspots than COs (with ~70% of NCO events occurring within PRDM9-positioned hotspots in humans; Baudat et al. 2013; Williams et al. 2015; Halldorsson et al. 2016; Palsson et al. 2025), the degenerate hotspot motif (Fig. 1b) was observed in each 10 kb region centered around a NCO event, providing support that these events are likely genuine rather than sequencing artifacts.

On average, 0.71 NCOs were identified per chromosome and meiosis, with 1 to 20 NCOs per meiosis across the 14 autosomes (supplementary table S8, Supplementary Material online). Although quantitatively similar to recent estimates in catarrhines (e.g. 1.06 NCOs per chromosome and meiosis in rhesus macaques [Versoza et al. 2024b] as well as 2.39/2.90 NCOs per chromosome and paternal/maternal meiosis in humans [Palsson et al. 2025]), this represents a conservative estimate, both because NCO events occurring between phase-informative markers will inevitably be missed (a particular challenge for species exhibiting low heterozygosity—and thus low marker density—such as aye-ayes) but also because the application of stringent quality metrics required to filter out false positives may have inadvertently removed genuine NCO events. Specifically, given an average of 517,832 phase-informative markers per pedigree/family (supplementary table S3, Supplementary Material online), markers are expected to occur roughly every 4,400 bp and thus, only a small subset of all genuine NCOs will be detectable in this dataset. To estimate the probability of a NCO event being detectable in the dataset on hand, 2,000 NCO events of varying length were simulated using the NCO length distribution recently reported for the best-studied primate, humans, as a reasonable proxy (Supplementary Table 4 in Palsson et al. 2025). As anticipated from the low marker density—and similar to a recent study of >5,000 human trios in which 2.3% (2.39 out of 105.0) and 3.6% (2.90 out of 81.6) of estimated NCO events per offspring were observed

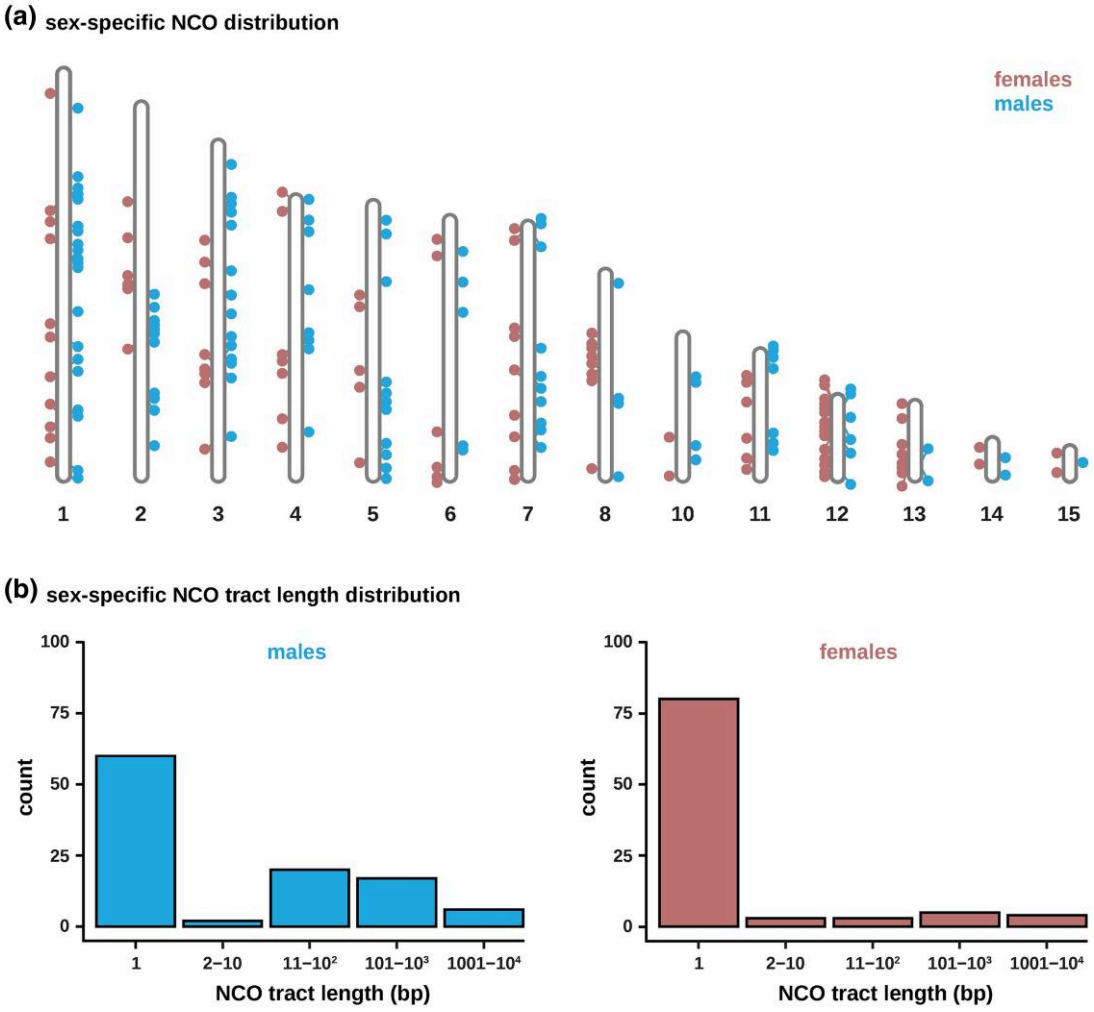


**Fig. 2. Characteristics of noncrossovers**. a) The genomic distribution of NCO events in females (shown as pink circles) and males (blue circles) across the autosomes (note that scaffold 9, i.e. chromosome X, is not displayed). b) Distribution of sex-specific NCO tract lengths (reported in base pairs [bp]) based on phase-informative sites that mismatched the surrounding haplotype block.

for paternal and maternal meioses, respectively (Palsson et al. 2025)—the probability of identifying NCO events is low for short tracts (2.5% on average) and higher for extended tracts (58.3%), suggesting that the genuine number of NCO events per meiosis is much higher. This difficulty of detecting NCOs from pedigree data is well-appreciated in the limited number of vertebrate studies in which such events have been investigated in depth (see e.g. the discussions in Williams et al. (2015), Smeds et al. (2016), and Palsson et al. (2025)); however, as such, the ratio of NCO:CO cannot be meaningfully compared in this study.

NCOs are slightly less abundant in females than males (8.6 vs. 9.6) and exhibit shorter average minimal tract lengths (157 vs. 163 bp; Fig. 2b and see supplementary table S8, Supplementary Material online)—an observation that might, at least in part, be driven by the lower density of phase-informative markers in females than in males in the two-generation nuclear families (though note that the difference in marker density is not statistically significant; two-sample $t$-test: $t = -2.4417$; df = 2.9396; $P$-value = 0.09412; supplementary table S3, Supplementary Material online). The sex-averaged mean minimal tract length of 161 bp is similar to those observed in pedigree studies of other primates (with estimated mean tract lengths of 55 to 290 bp in humans [Jeffreys and May 2004; Palsson et al. 2025], 42 to 167 bp in baboons [Wall et al. 2022], and 155 bp in rhesus macaques [Versoza et al. 2024b])—however, it should be noted that differences in marker density will impact resolution, rendering such comparisons across species challenging. In fact, similar to a previous pedigree-based study in humans (Williams et al. 2015), the majority of events (140 out of 200, or 70%) include only a single phase-informative marker, exhibiting a minimal tract length of 1 bp (note that no significant difference between the mutation spectra of the phase-informative

markers tagging NCO events, the phase-informative markers in the two-generation nuclear families, and the phase-informative markers in the three-generation pedigrees was observed; Kruskal–Wallis $\chi^2 = 0.013995$, df = 2, *P*-value = 0.993; and see supplementary table S11, Supplementary Material online). Events involving multiple phase-informative markers generally exhibited short minimal tract lengths (median: 136 bp; mean: 534 bp); however, similar to humans (Williams et al. 2015), baboons (Wall et al. 2022), and rhesus macaques (Versoza et al. 2024b), several NCOs with minimal tract lengths longer than 1 kb were also observed (6 in males and 4 in females; supplementary table S10, Supplementary Material online). Furthermore, in agreement with empirical patterns observed in other primates (Williams et al. 2015; Halldorsson et al. 2016; Wall et al. 2022; Versoza et al. 2024b; Palsson et al. 2025), the distribution of NCO minimal tract lengths (Fig. 2b) appears more consistent with a power-law (or heavy-tailed) distribution than the single geometric distribution frequently modeled (Frisse et al. 2001; Gay et al. 2007; Yin et al. 2009).

Based on the observed minimal tract lengths and an autosomal genome length of 2.28 Gb (supplementary tables S8 and S10, Supplementary Material online), aye-ayes exhibit a sex-averaged NCO rate of $6.8 \times 10^{-7}$ per base pair per generation (95% CI: $2.9 \times 10^{-7}$ to $1.1 \times 10^{-6}$/bp/gen), with similar rates between the sexes ($6.4 \times 10^{-7}$/bp/gen in females vs. $7.4 \times 10^{-7}$/bp/gen in males; Mann–Whitney *U* test, *P*-value = 0.38) and an expected average of ~1.5 kb of autosomal sequence affected by NCOs in each generation. The actual sex-averaged NCO rate is likely much greater given the small sample size and low marker density of this study and, taking the simulation results at face value, is likely closer to $2.3 \times 10^{-6}$/bp/gen, affecting an estimated ~50 kb per generation.

In summary, the landscape of CO and NCO events in aye-ayes presented here provides novel insights into a parameter crucial for improving population genetic modeling in this highly endangered species, and will serve as a valuable resource for future comparative genomic studies seeking to understand the long-term evolution of recombination landscapes across the primate clade.

## Materials and Methods

### Sequencing, Read Mapping, and Variant Calling

A total of 14 aye-aye individuals (eight females and six males) were selected from six three-generation pedigrees and three (partially overlapping) two-generation multi-sibling families available at the Duke Lemur Center, the genomes of which were sequenced to an average coverage of 50× per individual (supplementary table S1, Supplementary Material online). Sequencing reads were mapped to the aye-aye genome assembly (DMad_hybrid; GenBank accession number: GCA_044048945.1; Versoza and Pfeifer 2024) in order to call autosomal, biallelic single nucleotide polymorphisms (SNPs) genotyped in all individuals (see Versoza et al. (2025) for details regarding the autosomes and Terbot et al. (2025a) for a comparison with chromosome X). In the absence of a curated "gold standard" variant dataset that could serve as a basis for variant filtration in the species, initial calls were filtered using the Genome Analysis Toolkit's Best Practice "hard filter" criteria for germline variants (van der Auwera and O'Connor 2020). Following the methodology described by Versoza et al. (2024b), a set of additional coverage-, genotype-, and inheritance-based filters was applied to further increase the precision of the variant call set. Specifically, variants were excluded if (i) they were located within repetitive and low-complexity regions of the genome prone to base calling errors and mis-mappings (Pfeifer 2017), or if they exhibited (ii) a total depth of coverage (*DP*) of less than half or more than twice the average autosomal coverage for each sample, (iii) a genotype quality (*GQ*) less than 30 (corresponding to a probability of a genotyping error of more than $10^{-3}$), (iv) an excess of heterozygosity (defined here as a *P*-value of 0.01), and/or (v) violated the patterns expected by Mendelian inheritance (as determined using the BCFtools + *mendelian2* plugin [Danecek et al. 2021] together with the information of the pedigree). Additionally, to further reduce variant calling and/or genotyping errors that could potentially lead to spurious recombination events, SNPs located within either (i) a cluster of variants (defined here as ≥3 SNPs within a 10 bp window), (ii) 10 bp of an insertion/deletion, or (iii) 2 Mb from the chromosome ends, were also excluded from further analyses. The resulting high-confidence call set consisted of 1,830,431 SNPs with a transition–transversion ratio of 2.62 (supplementary table S2, Supplementary Material online).

### Identification of CO and NCO Events

The high-confidence call set was divided into six three-generation pedigrees and three (partially overlapping) two-generation nuclear families with multiple offspring (supplementary fig. S1, Supplementary Material online) for which gamete transmission could be tracked in order to identify recombination events based on "phase-informative" markers—that is, heterozygous SNPs for which the parent-of-origin could be determined (supplementary table S3, Supplementary Material online). In brief, in the three-generation pedigrees, phase-informative markers were sites at which the $P_0$ individuals exhibited nonidentical genotypes, their $F_1$ offspring was heterozygous, and either the $F_1$'s partner or their joint $F_2$ offspring was homozygous (for a schematic of the workflow, see Fig. 1b in Versoza et al. 2024b). In the two-generation nuclear families, maternally phase-informative markers exclusively included those for which the dam was heterozygous and the sire homozygous, whereas paternally phase-informative markers included

sites at which the sire was heterozygous and the dam homozygous. Following the methodology outlined in Coop et al. (2008), recombination events were then identified by comparing these phase-informative markers across siblings using a randomly assigned offspring as "template" (note that although recombination events can be identified in a single sibling pair using this approach, it is not possible to unequivocally assign the meiosis in which the event occurred; see supplementary fig. S20, Supplementary Material online for a schematic of the workflow). In both cases, heterozygous genotype calls in phase-informative markers required the support of more than 25% but less than 75% of mapped reads to limit genotyping errors in the downstream analyses.

Based on these phase-informative markers, recombination events were classified as either COs—that is, a single change of phase along a chromosome (from maternally inherited to paternally inherited haplotype blocks or vice versa, ignoring single phase-informative markers within a region of consistent phase)—or NCOs—that is, phase-informative markers that mismatched surrounding haplotype blocks. CO interference prevents the occurrence of two CO events in close proximity to each other (Otto and Payseur 2019), thus following Venn et al. (2014), a minimum distance of 1 Mb was required between two COs that originated from the same meiosis (see supplementary table S5, Supplementary Material online for a summary of the removed CO events). Similarly, following Smeds et al. (2016), to reduce the number of spurious NCO events resulting from genotyping errors, a minimum distance of 5 kb was required between two consecutive NCOs; additionally, complex NCO events longer than 10 kb were excluded from further analyses as previous work demonstrated that these frequently represent assembly errors (Wall et al. 2022). For the four meioses that could be studied using both the three-generation pedigree approach and the two-generation family approach (i.e. focal individual–offspring pairs 7–12, 7–13, 8–12, and 8–13; see supplementary fig. S1, Supplementary Material online), recombination events were manually consolidated. Notably, all CO events in these meioses were identified by both approaches, with the majority of events (54%) sharing identical start and end coordinates at the break point. In case of a partial overlap (i.e. a sharing of either start or end coordinates at the break point owing to different phase-informative markers in the two approaches), the CO events with the shortest resolution were selected. Shorter CO resolution tracts were generally observed using the pedigree-based approach (only 24% of events exhibited shorter resolutions in the family-based approach) due to a larger number of phase-informative markers (supplementary table S3, Supplementary Material online, and see supplementary table S4 and figs. S2 to S15, Supplementary Material online for the marker density across each autosome per pedigree/family). In contrast, due to the low density of markers and the short tract lengths, only 48 of the 120 NCO events (40%) were detected with both approaches. Of these, 83% exhibited identical break point coordinates; for the remaining, partially overlapping events, the NCOs with the longest length tract were selected. Lastly, to guard against assembly errors, CO and NCO events detected in more than one meiosis and those overlapping with structural variation (Versoza et al. 2024a) were removed (see supplementary tables S6 and S9, Supplementary Material online for COs and NCOs, respectively).

## Annotation

High-confidence COs (defined here as COs with a resolution shorter than 5 kb) and NCOs (with a tract length shorter than 5 kb) were classified by genomic region (i.e. intergenic, upstream, exonic, exonic noncoding RNA [ncRNA], intronic, intronic ncRNA, 3′ and 5′ UTR, and downstream) and repeat content using ANNOVAR v.2020-06-08 (Wang et al. 2010) together with information from the aye-aye genome annotation (Versoza and Pfeifer 2024). CO and NCO events were checked for overlap with structural variants cataloged in the individuals of this study (Versoza et al. 2024a). Statistics were calculated and plotted using R v.4.2.2 (R Core Team 2022). Ideograms of the genome-wide maps were plotted with RIdeogram v.0.2.2 (Hao et al. 2020).

## Motif Identification

CO events with a high resolution were leveraged to search for putative sequence motifs of PRDM9 binding sites in aye-ayes. Following Wijnker et al. (2013), the 110 CO regions with a resolution of less than 10 kb were extended to include the neighboring 500 bp in order to ensure that the complete region subject to double-strand break and repair was included, and the de novo motif finding algorithm implemented in MEME v.5.5.7 (Bailey and Elkan 1994) was run using the zero or one occurrence per sequence (ZOOPS) model. To account for potential nucleotide sequence bias, the search was corrected for genomic background using a model built from randomly selected nonbreakpoint regions with the same genomic characteristics (i.e. sequence length and GC content) as the breakpoint regions. Given that many human recombination hotspots harbor a degenerate 13-mer sequence motif (Myers et al. 2008), the search was limited to motifs with a minimum and maximum width of 5 and 15 bases, respectively. A single degenerate motif passed the discovery threshold of 1e-05. Similar to humans (Altemose et al. 2017), this degenerate motif is highly repetitive, and thus, a permutation test was performed to compare its distribution in breakpoint regions with that in nonbreakpoint regions. To this end, an additional 1,000 random nonbreakpoint regions were sampled and MOODS v.1.9.4.1 (Korhonen et al. 2009) was used to scan both breakpoint and nonbreakpoint regions for occurrences of the degenerate motif based on a positional weight matrix, considering matches with a $P$-value $< 0.05$. A Fisher's exact test was performed using R

v.4.2.2 (R Core Team 2022) to test for statistical significance of the observed differences.

### PRDM9–DNA Binding

In many primates, the location of recombination is mainly determined by the zinc-finger protein PRDM9 binding specific DNA sequence motifs (Baudat et al. 2010; Myers et al. 2010; Parvanov et al. 2010). In order to characterize PRDM9–DNA binding in silico, the nucleotide sequence of PRDM9 in aye-ayes was obtained from the recent genome annotation of the species (Versoza and Pfeifer 2024), visually checked for completeness and potential frameshift errors by alignment against the human PRDM9 protein sequence included in the Universal Protein Knowledgebase (UniProt Consortium 2025) using GeneWise v.2.4.1 (Birney et al. 2004), and translated into a protein sequence using the ExPASy web server (Appel et al. 1994; Gasteiger et al. 2003; Artimo et al. 2012; Duvaud et al. 2021). A BlastP (Altschul et al. 1990) search of the aye-aye PRDM9 protein sequence against the NCBI reference database demonstrated a high sequence similarity with PRDM9 in other primates (supplementary fig. S21, Supplementary Material online) and a multiple-sequence alignment with the PRDM9 protein sequence in humans provided evidence that the KRAB domain, the PR/SET domain, and the zinc-finger array are well-characterized (supplementary fig. S22, Supplementary Material online). The presence of these domains and the zinc-finger array in aye-ayes was additionally supported by the protein sequence classification obtained from InterPro (Blum et al. 2025) (supplementary fig. S23, Supplementary Material online). With both the PRDM9 protein sequence and a putative degenerate binding motif (see "Motif identification") on hand, AlphaFold 3 (Abramson et al. 2024) was used to predict PRDM9–DNA binding.

### Detectability of NCO Events

The detection of NCO events is complicated by both the short tract lengths and the need for a segregating variant to be present in the donor homolog in order to allow identification—a particular challenge for highly endangered species with low levels of heterozygosity and consequently low marker density. To estimate the probability of a NCO event being detectable in the aye-aye dataset on hand, 2,000 NCO events of varying length were simulated using the NCO length distribution recently reported for humans (Supplementary Table 4 in Palsson et al. 2025) as a reasonable proxy (as precise estimates of NCO tract lengths remain elusive in many species, including aye-ayes). Specifically, 500 maternal short NCO events were simulated based on a mean NCO length of 102 bp (95% CI: 71 to 125 bp), 500 paternal short NCO events were simulated based on a mean NCO length of 123 bp (95% CI: 94 to 135 bp), 500 maternal extended NCO events were simulated based on a mean NCO length of 9.1 kb (95% CI: 6.8 to 10.8 kb), and 500 paternal extended NCO events were simulated based on a mean NCO length of 7.2 kb (95% CI: 1.8 to 11.8 kb), and the number of NCO events containing at least one phase-informative marker was recorded. Power was calculated by dividing the number of detectable NCOs by the total number of simulated NCO events in each category, with sex-specific events combined as size differences between sexes were not significant in humans (Palsson et al. 2025).

## Supplementary Material

Supplementary material is available at *Genome Biology and Evolution* online.

## Acknowledgments

We would like to thank Erin Ehmke, Kay Welser, and the Duke Lemur Center for providing the aye-aye samples used in this study. DNA extraction, library preparation, and Illumina sequencing were conducted at Azenta Life Sciences (South Plainfield, NJ, USA). Computations were performed on the Sol supercomputer at Arizona State University (Jennewein et al. 2023). This is Duke Lemur Center publication # 1616.

## Funding

This work was supported by the National Institute of General Medical Sciences of the National Institutes of Health under Award Number R35GM151008 to S.P.P. and the National Science Foundation under Award Number DBI-2012668 to the Duke Lemur Center. C.J.V. was supported by the National Science Foundation CAREER Award DEB-2045343 to S.P.P. A.L.-V. was supported by the National Institutes of Health under Award Number R35GM151008 to S.P.P. J.D.J. was supported by the National Institute of General Medical Sciences of the National Institutes of Health under Award Number R35GM139383. The content is solely the responsibility of the authors and does not necessarily represent the official views of the National Institutes of Health or the National Science Foundation.

## Conflict of Interest

None declared.

## Data Availability

All sequence data have been deposited under NCBI BioProjects PRJNA1179987 and PRJNA1181251. Computational workflows for the detection of crossover and noncrossover events were implemented using Snakemake v.7.32.4 (Mölder et al. 2021) and are available via GitHub: https://github.com/PfeiferLab/aye-aye_CO_NCO.

## Literature Cited


Abramson J, Adler J, Dunger J, Evans R, Green T, Pritzel A, Ronneberger O, Willmore L, Ballard AJ, Bambrick J, et al. Accurate structure prediction of biomolecular interactions with AlphaFold 3. Nature. 2024:630(8016):493–500. https://doi.org/10.1038/s41586-024-07487-w.

Altemose N, Noor N, Bitoun E, Tumian A, Imbeault M, Chapman JR, Aricescu AR, Myers SR. A map of human PRDM9 binding provides evidence for novel behaviors of PRDM9 and other zinc-finger proteins in meiosis. eLife. 2017:6:e28383. https://doi.org/10.7554/eLife.28383.

Altschul SF, Gish W, Miller W, Myers EW, Lipman DJ. Basic local alignment search tool. J Mol Biol. 1990:215(3):403–410. https://doi.org/10.1016/S0022-2836(05)80360-2.

Appel RD, Bairoch A, Hochstrasser DF. A new generation of information retrieval tools for biologists: the example of the ExPASy WWW server. Trends Biochem Sci. 1994:19(6):258–260. https://doi.org/10.1016/0968-0004(94)90153-8.

Artimo P, Jonnalagedda M, Arnold K, Baratin D, Csardi G, de Castro E, Duvaud S, Flegel V, Fortier A, Gasteiger E, et al. ExPASy: SIB bioinformatics resource portal. Nucleic Acids Res. 2012:40(W1):W597–W603. https://doi.org/10.1093/nar/gks400.

Auton A, Fledel-Alon A, Pfeifer S, Venn O, Ségurel L, Street T, Leffler EM, Bowden R, Aneas I, Broxholme J, et al. A fine-scale chimpanzee genetic map from population sequencing. Science. 2012:336(6078):193–198. https://doi.org/10.1126/science.1216872.

Bailey TL, Elkan C. Fitting a mixture model by expectation maximization to discover motifs in biopolymers. Proc Int Conf Intell Syst Mol Biol. 1994:2:28–36.

Baudat F, Buard J, Grey C, Fledel-Alon A, Ober C, Przeworski M, Coop G, de Massy B. PRDM9 is a major determinant of meiotic recombination hotspots in humans and mice. Science. 2010:327(5967):836–840. https://doi.org/10.1126/science.1183439.

Baudat F, Imai Y, de Massy B. Meiotic recombination in mammals: localization and regulation. Nat Rev Genet. 2013:14(11):794–806. https://doi.org/10.1038/nrg3573.

Bhérer C, Campbell CL, Auton A. Refined genetic maps reveal sexual dimorphism in human meiotic recombination at multiple scales. Nat Commun. 2017:8(1):14994. https://doi.org/10.1038/ncomms14994.

Birney E, Clamp M, Durbin R. GeneWise and Genomewise. Genome Res. 2004:14(5):988–995. https://doi.org/10.1101/gr.1865504.

Blum M, Andreeva A, Florentino LC, Chuguransky SR, Grego T, Hobbs E, Pinto BL, Orr A, Paysan-Lafosse T, Ponamareva I, et al. InterPro: the protein sequence classification resource in 2025. Nucleic Acids Res. 2025:53(D1):D444–D456. https://doi.org/10.1093/nar/gkae1082.

Broman KW, Weber JL. Characterization of human crossover interference. Am J Hum Genet. 2000:66(6):1911–1926. https://doi.org/10.1086/302923.

Charlesworth B, Jensen JD. Effects of selection at linked sites on patterns of genetic variability. Annu Rev Ecol Evol Sys. 2021:52(1):177–197. https://doi.org/10.1146/annurev-ecolsys-010621-044528.

Cole F, Keeney S, Jasin M. Comprehensive, fine-scale dissection of homologous recombination outcomes at a hot spot in mouse meiosis. Mol Cell. 2010:39(5):700–710. https://doi.org/10.1016/j.molcel.2010.08.017.

Comeron JM, Ratnappan R, Bailin S. The many landscapes of recombination in *Drosophila melanogaster*. PLoS Genet. 2012:8(10):e1002905. https://doi.org/10.1371/journal.pgen.1002905.

Coop G, Wen X, Ober C, Pritchard JK, Przeworski M. High-resolution mapping of crossovers reveals extensive variation in fine-scale recombination patterns among humans. Science. 2008:319(5868):1395–1398. https://doi.org/10.1126/science.1151851.

Cox LA, Mahaney MC, Vandeberg JL, Rogers J. A second-generation genetic linkage map of the baboon (*Papio hamadryas*) genome. Genomics. 2006:88(3):274–281. https://doi.org/10.1016/j.ygeno.2006.03.020.

Danecek P, Bonfield JK, Liddle J, Marshall J, Ohan V, Pollard MO, Whitwham A, Keane T, McCarthy SA, Davies RM, et al. Twelve years of SAMtools and BCFtools. GigaScience. 2021:10(2):giab008. https://doi.org/10.1093/gigascience/giab008.

Duvaud S, Gabella C, Lisacek F, Stockinger H, Ioannidis V, Durinx C. Expasy, the Swiss Bioinformatics Resource Portal, as designed by its users. Nucleic Acids Res. 2021:49(W1):W216–W227. https://doi.org/10.1093/nar/gkab225.

Felsenstein J. The evolutionary advantage of recombination. Genetics. 1974:78(2):737–756. https://doi.org/10.1093/genetics/78.2.737.

Finelli P, Stanyon R, Plesker R, Ferguson-Smith MA, O'Brien PC, Wienberg J. Reciprocal chromosome painting shows that the great difference in diploid number between human and African green monkey is mostly due to non-Robertsonian fissions. Mamm Genome. 1999:10(7):713–718. https://doi.org/10.1007/s003359901077.

Frisse L, Hudson RR, Bartoszewicz A, Wall JD, Donfack J, Di Rienzo A. Gene conversion and different population histories may explain the contrast between polymorphism and linkage disequilibrium levels. Am J Hum Genet. 2001:69(4):831–843. https://doi.org/10.1086/323612.

Gasteiger E, Gattiker A, Hoogland C, Ivanyi I, Appel RD, Bairoch A. ExPASy: the proteomics server for in-depth protein knowledge and analysis. Nucleic Acids Res. 2003:31(13):3784–3788. https://doi.org/10.1093/nar/gkg563.

Gay J, Myers S, McVean G. Estimating meiotic gene conversion rates from population genetic data. Genetics. 2007:177(2):881–894. https://doi.org/10.1534/genetics.107.078907.

Gross M. Primates in peril. Curr Biol. 2017:27(12):R573–R576. https://doi.org/10.1016/j.cub.2017.06.002.

Halldorsson BV, Hardarson MT, Kehr B, Styrkarsdottir U, Gylfason A, Thorleifsson G, Zink F, Jonasdottir A, Jonasdottir A, Sulem P, et al. The rate of meiotic gene conversion varies by sex and age. Nat Genet. 2016:48(11):1377–1384. https://doi.org/10.1038/ng.3669.

Hao Z, Lv D, Ge Y, Shi J, Weijers D, Yu G, Chen J. RIdeogram: drawing SVG graphics to visualize and map genome-wide data on the idiograms. PeerJ Comput Sci. 2020:6:e251. https://doi.org/10.7717/peerj-cs.251.

Hill WG, Robertson A. The effects of linkage on limits to artificial selection. Genet Res. 1966:8(3):269–294. https://doi.org/10.1017/S0016672300010156.

Jasinska AJ, Service S, Levinson M, Slaten E, Lee O, Sobel E, Fairbanks LA, Bailey JN, Jorgensen MJ, Breidenthal SE, et al. A genetic linkage map of the vervet monkey (*Chlorocebus aethiops sabaeus*). Mamm Genome. 2007:18(5):347–360. https://doi.org/10.1007/s00335-007-9026-4.

Jeffreys AJ, May CA. Intense and highly localized gene conversion activity in human meiotic crossover hot spots. Nat Genet. 2004:36(2):151–156. https://doi.org/10.1038/ng1287.

Jennewein DM, Lee J, Kurtz C, Dizon W, Shaeffer I, Chapman A, Chiquete A, Burks J, Carlson A, Mason N, et al. The Sol supercomputer at Arizona State University. In: Practice and Experience in Advanced Research Computing 2023: computing for the common good (PEARC '23). New York (NY): Association for Computing Machinery; 2023. p. 296–301.

Johnston SE. Understanding the genetic basis of variation in meiotic recombination: past, present, and future. Mol Biol Evol. 2024:41(7):msae112. https://doi.org/10.1093/molbev/msae112.

Jones GH, Franklin FC. Meiotic crossing-over: obligation and interference. Cell. 2006:126(2):246–248. https://doi.org/10.1016/j.cell.2006.07.010.
Keeney S. Mechanism and control of meiotic recombination initiation. Cur Top Dev Biol. 2001:52:1–53. https://doi.org/10.1016/S0070-2153(01)52008-6.
Kong A, Gudbjartsson DF, Sainz J, Jonsdottir GM, Gudjonsson SA, Richardsson B, Sigurdardottir S, Barnard J, Hallbeck B, Masson G, et al. A high-resolution recombination map of the human genome. Nat Genet. 2002:31(3):241–247. https://doi.org/10.1038/ng917.
Kong A, Thorleifsson G, Gudbjartsson DF, Masson G, Sigurdsson A, Jonasdottir A, Walters GB, Jonasdottir A, Gylfason A, Kristinsson KT, et al. Fine-scale recombination rate differences between sexes, populations and individuals. Nature. 2010:467(7319):1099–1103. https://doi.org/10.1038/nature09525.
Korhonen J, Martinmäki P, Pizzi C, Rastas P, Ukkonen E. MOODS: fast search for position weight matrix matches in DNA sequences. Bioinformatics. 2009:25(23):3181–3182. https://doi.org/10.1093/bioinformatics/btp554.
Lenormand T, Dutheil J. Recombination difference between sexes: a role for haploid selection. PLoS Biol. 2005:3(3):e63. https://doi.org/10.1371/journal.pbio.0030063.
Li R, Bitoun E, Altemose N, Davies RW, Davies B, Myers SR. A high-resolution map of non-crossover events reveals impacts of genetic diversity on mammalian meiotic recombination. Nat Commun. 2019:10(1):3900. https://doi.org/10.1038/s41467-019-11675-y.
Lorenz A, Mpaulo SJ. Gene conversion: a non-Mendelian process integral to meiotic recombination. Heredity (Edinb). 2022:129(1):56–63. https://doi.org/10.1038/s41437-022-00523-3.
Louis EE, Sefczek TM, Randimbiharinirina DR, Raharivololona B, Rakotondrazandry JN, Manjary D, Aylward M., Ravelomandrato F. 2020. *Daubentonia madagascariensis*. The IUCN red list of threatened species. Version 2020.2; e.T6302A115560793. https://doi.org/10.2305/IUCN.UK.2020-2.RLTS.T6302A115560793.en.
Mittermeier RA, Hawkins F, Louis EE. Lemurs of Madagascar. 3rd ed. Crystal City (VA): Conservation International; 2010. ISBN 978-1-934151-23-5.
Mölder F, Jablonski KP, Letcher B, Hall MB, Tomkins-Tinch CH, Sochat V, Forster J, Lee S, Twardziok SO, Kanitz A, et al. Sustainable data analysis with Snakemake. F1000 Res. 2021:10:33. https://doi.org/10.12688/f1000research.29032.2.
Muller HJ. The mechanism of crossing-over. Am Nat. 1916:50(592):193–221. https://doi.org/10.1086/279534.
Myers S, Bottolo L, Freeman C, McVean G, Donnelly P. A fine-scale map of recombination rates and hotspots across the human genome. Science. 2005:310(5746):321–324. https://doi.org/10.1126/science.1117196.
Myers S, Bowden R, Tumian A, Bontrop RE, Freeman C, MacFie TS, McVean G, Donnelly P. Drive against hotspot motifs in primates implicates the PRDM9 gene in meiotic recombination. Science. 2010:327(5967):876–879. https://doi.org/10.1126/science.1182363.
Myers S, Freeman C, Auton A, Donnelly P, McVean G. A common sequence motif associated with recombination hot spots and genome instability in humans. Nat Genet. 2008:40(9):1124–1129. https://doi.org/10.1038/ng.213.
Otto SP, Payseur BA. Crossover interference: shedding light on the evolution of recombination. Annu Rev Genet. 2019:53(1):19–44. https://doi.org/10.1146/annurev-genet-040119-093957.
Owen NM, Lawce HJ, Olson SB. A new rhesus macaque karyotype based on human-rhesus synteny. J Assoc Genet Technol. 2016:42(4):178–179.
Paigen K, Petkov P. Mammalian recombination hot spots: properties, control and evolution. Nat Rev Genet. 2010:11(3):221–233. https://doi.org/10.1038/nrg2712.
Palsson G, Hardarson MT, Jonsson H, Steinthorsdottir V, Stefansson OA, Eggertsson HP, Gudjonsson SA, Olason PI, Gylfason A, Masson G, et al. Complete human recombination maps. Nature. 2025:639(8055):700–707. https://doi.org/10.1038/s41586-024-08450-5.
Pardo-Manuel de Villena F, Sapienza C. Recombination is proportional to the number of chromosome arms in mammals. Mamm Genome. 2001:12(4):318–322. https://doi.org/10.1007/s003350020005.
Parvanov ED, Petkov PM, Paigen K. PRDM9 controls activation of mammalian recombination hotspots. Science. 2010:327(5967):835. https://doi.org/10.1126/science.1181495.
Peñalba JV, Wolf JBW. From molecules to populations: appreciating and estimating recombination rate variation. Nat Rev Genet. 2020:21(8):476–492. https://doi.org/10.1038/s41576-020-0240-1.
Perry GH, Louis EE Jr, Ratan A, Bedoya-Reina OC, Burhans RC, Lei R, Johnson SE, Schuster SC, Miller W. Aye-aye population genomic analyses highlight an important center of endemism in northern Madagascar. Proc Natl Acad Sci U S A. 2013:110(15):5823–5828. https://doi.org/10.1073/pnas.1211990110.
Pfeifer SP. From next-generation resequencing reads to a high-quality variant data set. Heredity (Edinb). 2017:118(2):111–124. https://doi.org/10.1038/hdy.2016.102.
Pfeifer SP. A fine-scale genetic map for vervet monkeys. Mol Biol Evol. 2020:37(7):1855–1865. https://doi.org/10.1093/molbev/msaa079.
Pfeifer SP, Jensen JD. The impact of linked selection in chimpanzees: a comparative study. Genome Biol Evol. 2016:8(10):3202–3208. https://doi.org/10.1093/gbe/evw240.
Porubsky D, Dashnow H, Sasani TA, Logsdon GA, Hallast P, Noyes MD, Kronenberg ZN, Mokveld T, Koundinya N, Nolan C, et al. A familial, telomere-to-telomere reference for human de novo mutation and recombination from a four-generation pedigree. bioRxiv 606142. https://doi.org/10.1101/2024.08.05.606142, 5 August 2024, preprint: not peer reviewed.
Powers NR, Parvanov ED, Baker CL, Walker M, Petkov PM, Paigen K. The meiotic recombination activator PRDM9 trimethylates both H3K36 and H3K4 at recombination hotspots in vivo. PLoS Genet. 2016:12(6):e1006146. https://doi.org/10.1371/journal.pgen.1006146.
Pratto F, Brick K, Khil P, Smagulova F, Petukhova GV, Camerini-Otero RD. Recombination initiation maps of individual human genomes. Science. 2014:346(6211):1256442. https://doi.org/10.1126/science.1256442.
Przeworski M, Wall JD. Why is there so little intragenic linkage disequilibrium in humans? Genet Res. 2001:77(2):143–151. https://doi.org/10.1017/S0016672301004967.
R Core Team. R: a language and environment for statistical computing. Vienna, Austria: R Foundation for Statistical Computing; 2022. https://www.R-project.org/.
Rogers J, Garcia R, Shelledy W, Kaplan J, Arya A, Johnson Z, Bergstrom M, Novakowski L, Nair P, Vinson A, et al. An initial genetic linkage map of the rhesus macaque (*Macaca mulatta*) genome using human microsatellite loci. Genomics. 2006:87(1):30–38. https://doi.org/10.1016/j.ygeno.2005.10.004.
Rogers J, Mahaney MC, Witte SM, Nair S, Newman D, Wedel S, Rodriguez LA, Rice KS, Slifer SH, Perelygin A, et al. A genetic linkage map of the baboon (*Papio hamadryas*) genome based on human microsatellite polymorphisms. Genomics. 2000:67(3):237–247. https://doi.org/10.1006/geno.2000.6245.
Sardell JM, Kirkpatrick M. Sex differences in the recombination landscape. Am Nat. 2020:195(2):361–379. https://doi.org/10.1086/704943.

Smeds L, Mugal CF, Qvarnström A, Ellegren H. High-resolution mapping of crossover and non-crossover recombination events by whole-genome re-sequencing of an avian pedigree. PLoS Genet. 2016:12(5): e1006044. https://doi.org/10.1371/journal.pgen.1006044.

Soni V, Terbot JW, Versoza CJ, Pfeifer SP, Jensen JD. A whole-genome scan for evidence of positive and balancing selection in aye-ayes (*Daubentonia madagascariensis*) utilizing a well-fit evolutionary baseline model. G3 (Bethesda). 2025:jkaf078. https://doi.org/10.1093/g3journal/jkaf078.

Soni V, Versoza CJ, Terbot JW, Jensen JD, Pfeifer SP. Inferring fine-scale mutation and recombination rate maps in aye-ayes (*Daubentonia madagascariensis*). bioRxiv 2024.12.28.630620. https://doi.org/10.1101/2024.12.28.630620, 28 December 2024, preprint: not peer reviewed.

Stapley J, Feulner PGD, Johnston SE, Santure AW, Smadja CM. Variation in recombination frequency and distribution across eukaryotes: patterns and processes. Philos Trans R Soc Lond B Biol Sci. 2017:372(1736): 20160455. https://doi.org/10.1098/rstb.2016.0455.

Stevison LS, Woerner AE, Kidd JM, Kelley JL, Veeramah KR, McManus KF; Great Ape Genome Project; Bustamante CD, Hammer MF, Wall JD. The time scale of recombination rate evolution in great apes. Mol Biol Evol. 2016:33(4):928–945. https://doi.org/10.1093/molbev/msv331.

Suzzi-Simmons A. Status of deforestation of Madagascar. Glob Ecol Conserv. 2023:42:e02389. https://doi.org/10.1016/j.gecco.2023.e02389.

Tattersall I. The primates of Madagascar. New York: Columbia University Press; 1982.

Terbot JW, Soni V, Versoza CJ, Milhaven M, Calahorra-Oliart A, Shah D, Pfeifer SP, Jensen JD. 2025a. Interpreting patterns of X chromosomal relative to autosomal diversity in aye-ayes (*Daubentonia madagascariensis*). bioRxiv 634876. https://doi.org/10.1101/2025.01.25.634876, 27 January 2025, preprint: not peer reviewed.

Terbot JW, Soni V, Versoza CJ, Pfeifer SP, Jensen JD. Inferring the demographic history of aye-ayes (*Daubentonia madagascariensis*) from high-quality, whole-genome, population-level data. Genome Biol Evol. 2025b:17(1):evae281. https://doi.org/10.1093/gbe/evae281.

UniProt Consortium. UniProt: the Universal Protein Knowledgebase in 2025. Nucleic Acids Res. 2025:53(D1):D609–D617. https://doi.org/10.1093/nar/gkae1010.

van der Auwera GA, O'Connor BD. Genomics in the cloud: using Docker, GATK, and WDL in Terra. Sebastopol: O'Reilly Media; 2020.

Venn O, Turner I, Mathieson I, de Groot N, Bontrop R, McVean G. Strong male bias drives germline mutation in chimpanzees. Science. 2014:344(6189):1272–1275. https://doi.org/10.1126/science.344.6189.1272.

Versoza CJ, Ehmke EE, Jensen JD, Pfeifer SP. Characterizing the rates and patterns of de novo germline mutations in the aye-aye (*Daubentonia madagascariensis*). Mol Biol Evol. 2025:42(3): msaf034. https://doi.org/10.1093/molbev/msaf034.

Versoza CJ, Jensen JD, Pfeifer SP. 2024a. The landscape of structural variation in aye-ayes (*Daubentonia madagascariensis*). bioRxiv 622672. https://doi.org/10.1101/2024.11.08.622672, 11 November 2024, preprint: not peer reviewed.

Versoza CJ, Pfeifer SP. A hybrid genome assembly of the endangered aye-aye (*Daubentonia madagascariensis*). G3 (Bethesda). 2024:14(10):jkae185. https://doi.org/10.1093/g3journal/jkae185.

Versoza CJ, Weiss S, Johal R, La Rosa B, Jensen JD, Pfeifer SP. Novel insights into the landscape of crossover and noncrossover events in rhesus macaques (*Macaca mulatta*). Genome Biol Evol. 2024b:16(1):evad223. https://doi.org/10.1093/gbe/evad223.

Walker M, Billings T, Baker CL, Powers N, Tian H, Saxl RL, Choi K, Hibbs MA, Carter GW, Handel MA, et al. Affinity-seq detects genome-wide PRDM9 binding sites and reveals the impact of prior chromatin modifications on mammalian recombination hotspot usage. Epigenetics Chromatin. 2015:8(1):31. https://doi.org/10.1186/s13072-015-0024-6.

Wall JD, Robinson JA, Cox LA. High-resolution estimates of crossover and noncrossover recombination from a captive baboon colony. Genome Biol Evol. 2022:14(4):evac040. https://doi.org/10.1093/gbe/evac040.

Wang K, Li M, Hakonarson H. ANNOVAR: functional annotation of genetic variants from high-throughput sequencing data. Nucleic Acids Res. 2010:38(16):e164. https://doi.org/10.1093/nar/gkq603.

Wang S, Zickler D, Kleckner N, Zhang L. Meiotic crossover patterns: obligatory crossover, interference and homeostasis in a single process. Cell Cycle. 2015:14(3):305–314. https://doi.org/10.4161/15384101.2014.991185.

Wijnker E, Velikkakam James G, Ding J, Becker F, Klasen JR, Rawat V, Rowan BA, de Jong DF, de Snoo CB, Zapata L, et al. The genomic landscape of meiotic crossovers and gene conversions in *Arabidopsis thaliana*. eLife. 2013:2:e01426. https://doi.org/10.7554/eLife.01426.

Williams AL, Genovese G, Dyer T, Altemose N, Truax K, Jun G, Patterson N, Myers SR, Curran JE, Duggirala R, et al. Non-crossover gene conversions show strong GC bias and unexpected clustering in humans. eLife. 2015:4:e04637. https://doi.org/10.7554/eLife.04637.

Xue C, Raveendran M, Harris RA, Fawcett GL, Liu X, White S, Dahdouli M, Rio Deiros D, Below JE, Salerno W, et al. The population genomics of rhesus macaques (*Macaca mulatta*) based on whole-genome sequences. Genome Res. 2016:26(12):1651–1662. https://doi.org/10.1101/gr.204255.116.

Xue C, Rustagi N, Liu X, Raveendran M, Harris RA, Venkata MG, Rogers J, Yu F. Reduced meiotic recombination in rhesus macaques and the origin of the human recombination landscape. PLoS One. 2020:15(8):e0236285. https://doi.org/10.1371/journal.pone.0236285.

Yin J, Jordan MI, Song YS. Joint estimation of gene conversion rates and mean conversion tract lengths from population SNP data. Bioinformatics. 2009:25(12):i231–i239. https://doi.org/10.1093/bioinformatics/btp229.

**Associate editor**: Katerina Guschanski